ELSEVIER

Journal of Power Sources 55 (1995) 159–166

JOURNAL OF POWER SOURCES

Investigation of a carbon-supported quaternary Pt–Ru–Sn–W catalyst for direct methanol fuel cells

A.S. Aricò [a], Z. Poltarzewski [b], H. Kim [c], A. Morana [a], N. Giordano [a], V. Antonucci [a]

[a] *Institute CNR-TAE, Salita S. Lucia sopra Contesse 39, 98126 S. Lucia, Messina, Italy*

[b] *Department of Chemistry, Warsaw University of Technology, ul. Noakowskiego 3, 00-664 Warsaw, Poland*

[c] *Department of Chemistry, Seoul National University, Seoul 151-742, South Korea*

Received 24 July 1994; in revised form 6 August 1994; accepted 24 December 1994

Abstract

An investigation was carried out in the electro-oxidation of methanol on a carbon-supported quaternary Pt–Ru–Sn–W catalyst prepared by a liquid-phase reduction method. As derived by X-ray diffraction and X-ray photoelectron spectroscopy, the catalyst was composed of metallic Pt, microcrystalline RuO_2 and SnO_2 phases and amorphous WO_3/WO_2 species. The electrochemical analysis was carried out in half-cell containing sulfuric acid electrolyte as well as in a liquid methanol-fed solid polymer electrolyte single-cell. The activity of catalyst in the half-cell varied as a function of the methanol concentration, it increased with CH_3OH molarity in the activation-controlled region and showed a maximum in 2 M CH_3OH at high currents. *IR*-free polarization curves showed that the activity of the quaternary catalyst was superior to Pt metal/C samples having the same Pt amount. The presence of semi-insulating metal oxides such as RuO_2, SnO_2 and WO_3 on the electrode surface exhibited a significant uncompensated resistance. The single-cell performance was lower than that predicted by the half-cell experiments mainly due to the methanol cross-over through the Nafion membrane.

Keywords: Methanol fuel cells; Catalysts; Carbon; Platinum; Ruthenium; Tin; Tungsten

1. Introduction

The development of a liquid-fed fuel cell is a universal challenge as it would provide a system with more energy per unit volume and possibly be more apt for transportation in contrast to the hydrogen consuming devices. Electrochemical oxidation of liquid fuel to CO_2 removes the need for an external reformer and offers the prospect of producing compact systems ranging from a few watts up to several kilowatts. The potential market for direct methanol fuel cells (DMFCs) is not only an alternative to batteries but also as an independent power generator where a high power demand exists. In the longer term, DMFC could play a role as the most ideal power source for vehicle propulsion with lower costs at lower temperatures and higher energy density. Methanol is a very attractive fuel as it is abundant, relatively cheap, and it can be handled and distributed to the consumer through the present distribution services for petrol products. The main drawbacks limiting the practical realization of a commercially viable DMFC are poisoning of the catalyst by carbonaceous residues produced during the electro-oxidation of methanol and the cross-over of the liquid fuel through the electrolyte [1–9]. The electrocatalytic activity of Pt is known to be promoted by the presence of a second metal, such as Ru or Sn. The mechanism by which the synergistic promotion of the methanol oxidation reaction is brought about has been largely investigated [10–16]. It is generally accepted that an active catalyst for the methanol oxidation should give rise to a water displacement at lower potentials and to a 'labile' CO chemisorption.

It has been recently claimed that tungsten oxide was a suitable promoter of Pt towards the oxidation of methanol showing a significant decrease in the amount of poisoning species compared with Pt when it was used alone [17,18]. The presence of a 'spillover effect', caused by the formation of hydrogen tungsten bronze H_xWO_3 during the dehydrogenation process of methanol, was postulated [17,18].

The oxidation of methanol evolves through various stages, i.e., dehydrogenation, chemisorption of CO-like species, adsorption of OH species, chemical interaction between the adsorbed CO and OH compounds, and CO_2 evolution [7,8]. One of these stages may behave as the rate-determining step (rds) according to the

SSDI 0378-7753(94)02178-J

particular catalyst surface. The approach of a multifunctional catalyst is to increase simultaneously the rate of the various stages avoiding one of them becoming the rate-limiting process.

The present study is devoted to the investigation of the electrochemical behaviour of a quaternary Pt–Ru–Sn–W/C catalyst-based gas-diffusion fuel cell anode towards methanol oxidation both in half-cell and single-cell configurations. The nature of the active species on the catalyst has been studied employing X-ray diffraction (XRD) and X-ray photoelectron spectroscopy (XPS).

2. Experimental

2.1. Preparation and characterization of the catalysts

Carbon-supported Pt–Ru–Sn–W/C catalysts were obtained by liquid-phase reduction of chloroplatinic acid, tin chloride, ruthenium chloride and ammonium metatungstate precursors with sodium borohydride in an acidic solution. Ketjen black–EC carbon (2.5 g) was suspended in 100 ml of water at 80 °C. An aqueous solution (50 ml) containing 1 g Pt equivalent chloroplatinic acid and appropriate amounts of $(NH_4)_6H_2W_{12}O_{40}$, $SnCl_2$ and $RuCl_3$ in a hydrochloric acid solution (Pt:Ru:Sn:W molar ratio equal to 3:1:1:1) were added slowly to the carbon suspension and allowed for complete impregnation (lasting over 1 h). Reduction was performed by dropwise addition of 60 ml of 0.2 M $NaBH_4$. The slurry was maintained at 80 °C for 3 h to allow complete reduction of Pt and precipitation of metallic oxides. Subsequently, it was filtered, and washed copiously with hot distilled water to remove chloride ions. The filtrate solution was analysed by a Hitachi UV-Vis spectrophotometer in the range between 800 and 200 nm. The catalyst was dried in an air oven at 110 °C for 4 h. A few aliquots of the catalyst were heat-treated at 360 °C and at 450 °C for 20 min before XRD and XPS analyses. The composition of the metallic compounds in the quaternary catalyst after the heat treatment at 360 °C was Pt=18.3%, Ru=3.1%. Sn=3.6%, and W=5.6%.

2.2. X-ray diffraction

XRD patterns of the as-prepared Pt–Ru–Sn–W/C and thermal-treated catalysts were recorded on a Philips X Pert PW3710 X-ray powder diffractometer using Cu Kα radiation source. Thermal treatment was carried out in air at 360 °C for 20 min, in order to keep the conditions akin to the electrode preparation, and at 450 °C for 20 min to allow a better crystallization of the oxide phases.

2.3. X-ray photoelectron spectroscopy

The XPS measurements were performed using a VSW Scientific Instruments spectrometer (Manchester, UK); X-ray source was Al Kα at a power of 150 W. Spectra were obtained with pass energy of 90 eV for wide scans and 44 eV per individual elements. The pressure in the base chamber of the spectrometer was 5×10^{-10} mbar (Ti sublimation pump) and 5×10^{-9} mbar during the measurements. The XPS samples were prepared by coating the catalysts on sample holders (stainless steel 304), and drying at 100 °C in a low pressure (0.1 atm) oven for 1 h. The samples were introduced into the spectrometer using a separate differentially pumped fast entry chamber, then into a desorption chamber in ultrahigh vacuum for desorption of high volatile species adsorbed on carbon support, and finally into the analyser chamber. The background correlation was performed by Shirley method [19] and curve fitting by Gauss–Lorentz routines. The quantitative evaluation of each peak was obtained by dividing the integrated peak area by atomic sensitivity factors which were calculated from the ionization cross sections, the mean free electron escape depth and the measured transmission functions of spectrometer expressed as the relative intensity ratio to carbon [20,21].

2.4. Preparation and characterization of the electrodes

Dual-layer gas-diffusion electrodes were prepared for the investigation of the electrochemical oxidation of methanol at 60 °C in 0.5 M sulfuric acid. These comprised of a Pt–Ru–Sn–W catalyst or Pt/metal catalysts deposited on to a wet-proofed carbon cloth acting as a diffusion layer for the removal of CO_2 produced during the oxidation of methanol. The electrodes were prepared by first mixing the catalysts with water at 60 °C in an ultrasonic bath with mechanical stirring for about 30 min. Subsequently, a suspension of polytetrafluoroethylene (PTFE) (20 w/w %) was added dropwise to the catalyst and the slurry was further agitated for 30 min. An appropriate amount of isopropyl alcohol was added and the slurry was left to wet for 2 h. The flocculate was spread by doctor-blade technique over a Stackpole carbon cloth (Stackpole Fibers company, Lowell, MA, USA) wet-proofed with PTFE solution. The electrodes were pressed at 70 °C under 30 kg cm^{-2} for 1 h, then dried in an air oven at 110 °C for 1 h followed by heat treatment in the same oven at 360 °C for 20 min in air. The Pt loading in the electrodes was 0.8 mg cm^{-2}. The half-cell apparatus consisted of a water-thermostatted (60 °C) three-electrode cell. Gas-diffusion electrodes were mounted into a Teflon holder containing a Pt ring current collector. The electrode area exposed to the electrolyte was 1.5 cm^2. A large area Pt gauze was used as the counter electrode. An

AMEL saturated calomel reference electrode (+242 mV versus normal hydrogen electrode (NHE)) was placed in an external compartment filled with the same electrolyte and connected to the main body with a Luggin capillary whose tip was placed appropriately close to the working electrode. The electrode potentials were related to the NHE. The electrochemical cell was connected to a Tacussel PJT potentiostat/galvanostat. Steady-state galvonostatic measurements at various catalysed electrodes were performed manually. The uncompensated resistances (R_u) were measured by the current-interrupter method using a Philips memory oscilloscope.

2.5. Single cell

A Nafion membrane (Nafion 117, Du Pont de Nemours) was purified by immersion in a boiling 5% w/o H_2O_2/H_2O solution rinsed with bidistilled water, immersed in diluted H_2SO_4 at 80 °C and washed with boiling bidistilled water. Membrane and electrode assemblies were prepared according to Ref. [22]. The cathode was a commercial Prototech gas-diffusion electrode (0.35 mg Pt cm^{-2}). A 5% Nafion solution (Nafion 117, Solution Technology, Inc.) was spread on to the electrode surface to form a film (0.6 mg Nafion per cm^2) after solvent evaporation by drying in vacuum for 1 h at 70 °C. The Pt–Ru–Sn–W/C catalyst-based anode and a Pt/C cathode both coated with Nafion gel were hot-pressed on both sides of a Nafion membrane at 100 °C and 1 atm for 5 min and thereafter at 130 °C and 50 atm for 90 s followed by rapid cooling to room temperature. The electrode-membrane assembly was loaded into a single-cell test system allowing the passage of humidified oxygen at the cathode. A 2 M liquid methanol solution was fed at the anode and recirculated with a liquid pump. No preheating was used for the anolyte. The GlobeTech GT60 fuel cell test station (GlobeTech, Inc., Bryan, TX, USA), equipped with humidifiers, electronic load (HP 6060B), data acquisition system and controlled by an IBM PC, was used to drive all measurements. The water in the oxygen humidifier was maintained at a temperature 5 °C higher than the cell temperature. Uncompensated resistance was measured by an impedance bridge.

3. Results and discussion

The variations of the redox potential and pH versus the volume of the impregnating solution have been recorded in situ during the preparation of the catalyst [23]. As expected, the pH decreased upon addition of acidic metallic precursors to the carbon slurry whereas the potential increased to reach a constant value (0.76 V versus NHE) (Fig. 1). During the reduction of the

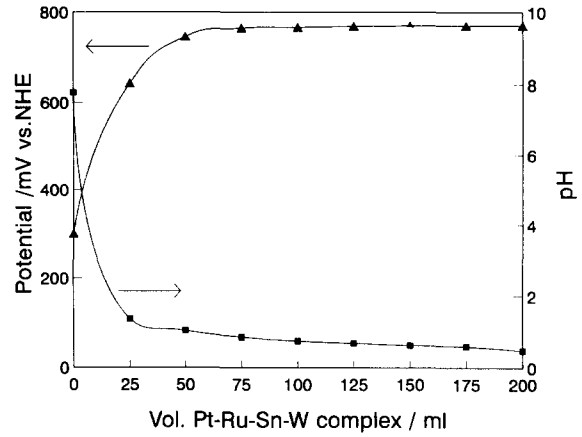

Fig. 1. Potential and pH versus volume of impregnating solution (16.9 mM H_2PtCl_6, 5.44 mM $RuCl_3$, 5.45 mM $SnCl_2$, 0.45 mM $(NH_4)_6H_2W_{12}O_{40}$) during the impregnation of carbon black.

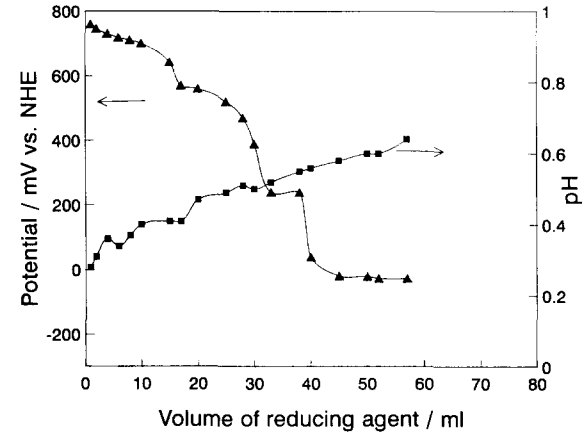

Fig. 2. Variations in potential and pH during the reduction process in the preparation of the Pt–Ru–Sn–W/C catalyst.

catalyst precursors with $NaBH_4$ (Fig. 2), the potential decreased in several steps, due to the presence of various redox systems to reach a steady-state value (−0.05 V versus NHE) corresponding to hydrogen evolution. From the Pourbaix diagrams [24], Pt and Ru should be present in a metallic state in the final conditions ($E = -0.05$ V versus NHE and pH = 0.6) whereas Sn and W are in an oxidized form. Tungsten is expected to precipitate as hydrate tungsten oxides (e.g., $WO_3 \cdot 2H_2O$ and $WO_2 \cdot H_2O$) or tungstic acid (H_2WO_4). Spectrophotometric analyses showed that this precipitation required several hours to be completed (disappearance of tungstate UV absorption band at 262 nm). The pH was found to increase during the reduction process. This effect is probably due to the precipitation of H_2WO_4 or related compounds. H^+ consumption prevails over both OH^- diminution due to reduction processes and H_2PtCl_6 decomposition [23].

XRD patterns of the as-prepared and the 360 °C treated catalysts showed the presence of crystalline Pt particles (Fig. 3). An average particle size of 60 Å was

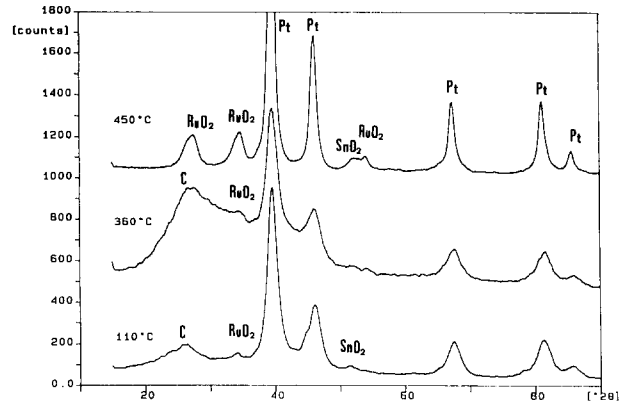

Fig. 3. X-ray diffraction patterns of the Pt–Ru–Sn–W/C catalyst: (a) as-prepared; (b) after heating in air at 360 °C, and (c) after heating in air at 450 °C for 20 min. C indicates the graphite peak.

determined by using the Debye–Scherrer equation. The small intensity peaks observed in the diffraction patterns at 2θ values comprised between 15° and 60° were assigned to graphite, RuO_2 and SnO_2. Yet, the broadening of these peaks accounts for the presence of a microcrystalline structure. RuO_2 and SnO_2 peaks increased in intensity and became narrower after heating the sample at 450 °C in air (Fig. 3). Diffraction peaks related to WO_3 or WO_2 were not detected. As the maximum T of 360 °C was reached during the preparation of the electrodes, it was observed that the electrodes contain crystalline Pt particles, microcrystalline RuO_2 and SnO_2 compounds and amorphous tungsten oxide.

The nature of surface species on the Pt–Ru–Sn–W/C catalyst heat-treated at 360 °C was investigated by XPS. The XP spectra of the Pt–Ru–Sn–W/C catalysts are shown in Fig. 4(a)–(f). The results are given in Table 1. The large C 1s signal (Fig. 4(a)) from carbon support at about 284.6 eV, superimposes to the Ru $3d_{3/2}$ line averting the investigation of oxidized Ru species in this region (RuO_2 binding energy is 284 eV). Ru $3d_{5/2}$ line in zero-valent Ru should be observed at 280 eV [25]. The absence of the metallic Ru peak in this region probably indicates that Ru is in an oxidized form on the catalyst surface. The C 1s spectra (Table 1) appear to be composed by graphitic carbon (284.6 eV) and −C=O (285.8 eV) species [26]. O 1s spectra are shown in Fig. 4(b). The O 1s signal is composed of three components. The peak occurring at 531.5 eV (Table 1) has a binding energy of 2 eV higher than the values reported in the literature for RuO_2 and SnO_2 and 1 eV higher than that of WO_3 [26]. Yet, the O 1s line at 531.5 eV can only be derived from these metallic oxides, the shift in the binding energy occurs due to a charging effect determined by the semi-insulating behaviour of the compounds. Furthermore, a small contribution could be due to the Pt-O like species (530 eV) and Pt–OH_{ads} species (531.5 eV) [27].

Table 1
Binding energy and relative intensities of different species from curve fitted X-ray photoelectron spectra in a Pt–Ru–Sn–W/C catalyst

Species	Binding energies (eV)		Relative intensity (%)
C 1s	284.6		82.4
	285.8		17.6
O 1s	531.5		52.3
	533.5		36.9
	534.8		10.8
Sn 3d	$3d_{5/2}$	$3d_{3/2}$	
	488.6	497.0	100
W 4f	$4f_{7/2}$	$4f_{5/2}$	
	34.70	36.85	41.2
	35.75	37.90	58.8
Pt 4f	71.03	74.38	87.6
	72.80	76.15	12.4
Ru 3p	$3p_{3/2}$	$3p_{1/2}$	100
	463.5	486.0	

The peaks obtained at higher binding energies are derived from the carbon functionalities (Table 1). The signal at 533.5 eV is ascribed to −C=O or ether-like species [26] whereas the high binding energy peak at 534.8 eV is due to carboxylic or ester-like functional groups. The Pt 4f signal is derived from two pairs of Pt peaks (Fig. 4(c)). The most intense peaks (71–74 eV) are attributed to metallic Pt. The second set of doublets occurring at a binding energy of 2 eV higher than Pt(O) can be assigned to Pt(II) state in PtO- and $Pt(OH)_2$-like species [28]. The Sn 4f spectra (Fig. 4(d)) are composed of only one pair of peaks at binding energies of 488.6 ($3d_{5/2}$) and 497 eV ($3d_{3/2}$). This accounts for the presence of SnO_2 species on the surface even if the Sn 3d peaks are shifted to higher binding energies by 1 eV [26], due to the charging effect. It is interesting to observe that the W 4f signal (Fig. 4(e)) is composed of two pairs of doublets at binding energies of 34.7 and 35.75 eV (W $4f_{7/2}$ line) and at 36.85 and 37.9 eV (W $4f_{5/2}$ line). These peaks are ascribed to the oxidation states (W(IV) and W(VI). They can be related to the presence of WO_2 and WO_3 species, respectively [26]. Yet, the W $4f_{7/2}$ signal at 34.7 eV may also be derived from the presence of W_2O_5 or substoichiometric WO_{3-x} ($2<x<3$) species. These tungsten oxides have comparable surface concentrations, i.e., WO_3 (59%) and WO_2 (41%), with a small prevalence of WO_3. It is expected that the WO_3/WO_2 system can act as a redox surface mediator for the oxidation of adsorbed methanolic residues. In fact, the redox potentials of these systems, calculated from the free energies, fall in the potential region where tungsten oxides redox couples may be active for methanol oxidation [29]:

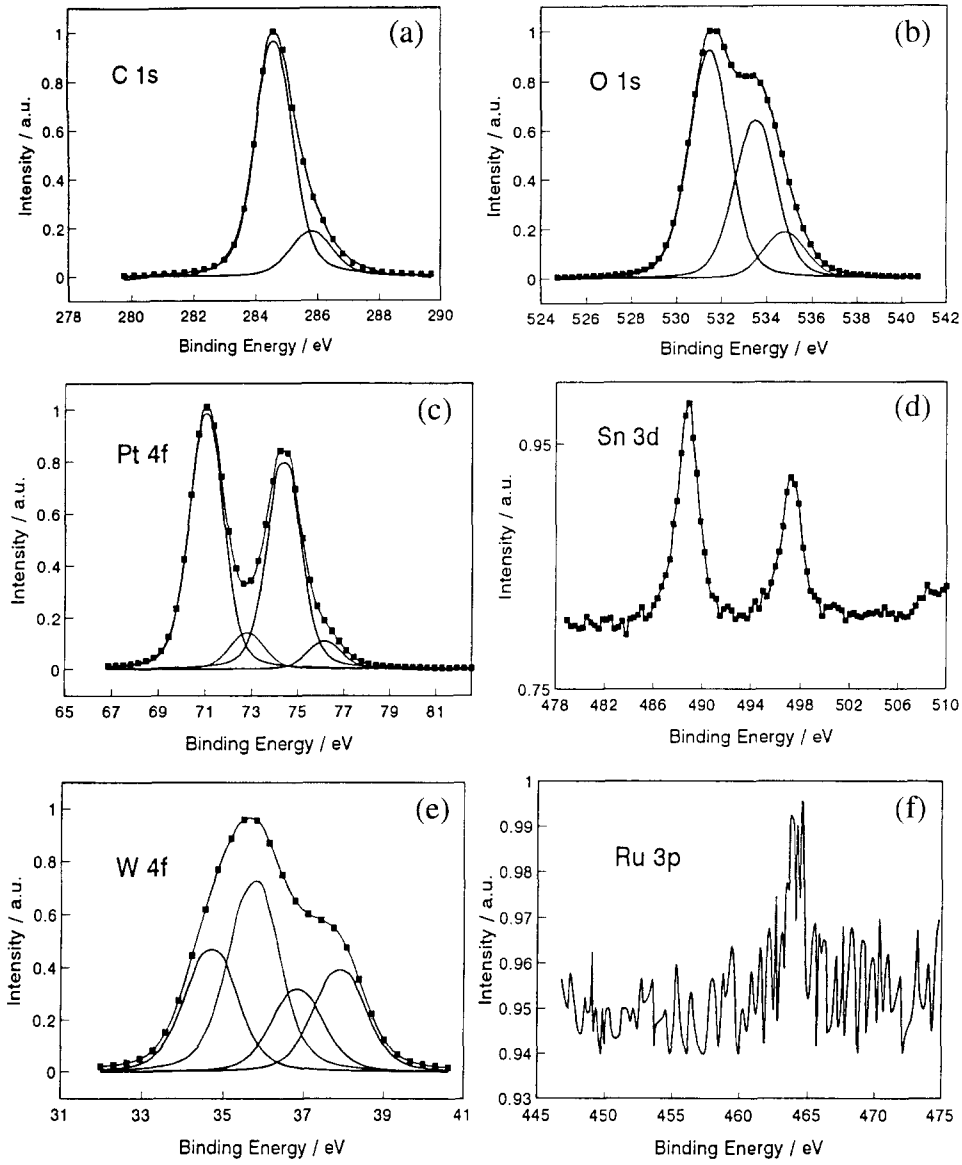

Fig. 4. (a)–(f) X-ray photoelectron spectra of the 360 °C treated Pt–Ru–Sn–W/C catalyst. The experimental spectra are shown by dots and fitted spectra by lines.

$$2WO_3(s) + 2H^+ + 2e^- \longrightarrow W_2O_5(s) + H_2O$$
$$E = +0.03 \text{ (NHE)} \quad (1)$$

$$W_2O_5(s) + 2H^+ + 2e^- \longrightarrow 2WO_2(s) + H_2O$$
$$E = +0.043 \text{ (NHE)} \quad (2)$$

Yet, due to the higher surface concentration of WO_3 species, it is likely that the tungsten oxide redox couples are operating at potentials higher than those corresponding to the thermodynamic data.

The Ru 3p signal for the Pt–Ru–Sn–W/C catalyst was scarcely resolved even after 20 scans of data collection (Fig. 4(f)). Furthermore, the Ru $3p_{1/2}$ line overlaps the large Sn 3d signal appearing as a shoulder at 486 eV (Fig. 4(d)). Although a clear identification of the oxidation state of Ru sites is not possible from this spectrum, a small Ru $3p_{3/2}$ peak observed at 463.5 eV (Fig. 4(f)) probably accounts for the presence of Ru(IV) oxide species on the catalyst surface [2].

Fig. 5 shows the galvanostatic current–potential data for the oxidation of methanol on Pt–Ru–Sn–W/C electrodes at various methanol concentrations together with their respective least-square regression curves. The latter allowed the analytical derivation of the limiting current density, I_l [30]. The lowest rest potential was observed in a 5 M CH_3OH solution and the catalytic activity increased in the activation region with the increase of the methanol concentration. Yet, the electrode tested in 2 M CH_3OH was found to be less polarized at high currents. The uncompensated resistance was obtained by the current-interrupt methods as well as by the linear regression of the dE/dI versus $1/I$ curves (Fig. 6) in the region where the limiting

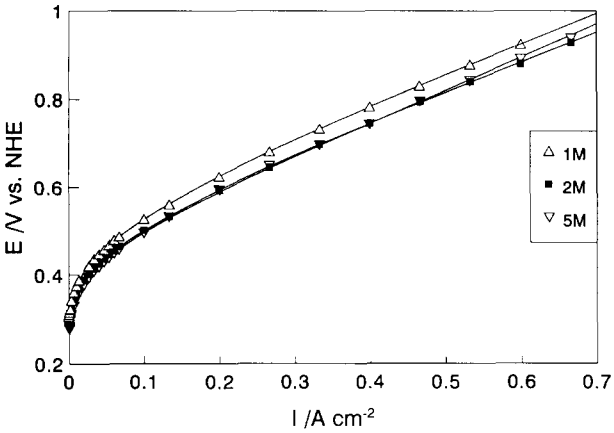

Fig. 5. Galvanostatic–polarization curves for the oxidation of methanol in 0.5 M H_2SO_4 at 60 °C at Pt–Ru–Sn–W/C electrodes.

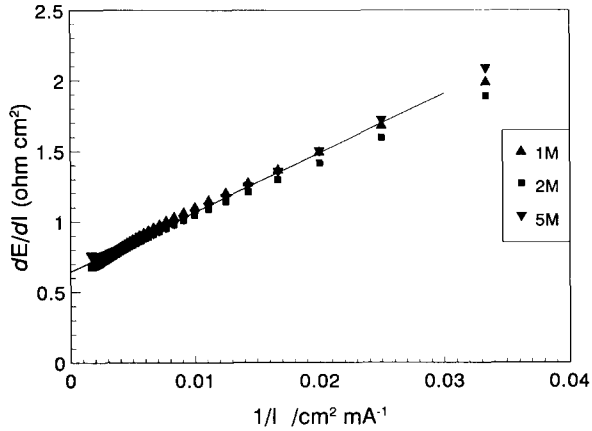

Fig. 6. dE/dI vs. 1/I obtained from polarization data in Fig. 5.

diffusion current does not significantly influence the data [31]. Results of the two methods are reported in Table 2. In the dE/dI versus 1/I plots, the intersect of the straight line (Fig. 6) gave the uncompensated resistance, whereas the linear increase of dE/dI versus 1/I function represented the contribution of the charge-transfer resistance to the electrode polarization [31]. The *IR*-free polarization curves of Pt–Ru–Sn–W/C in various CH_3OH concentrations are shown in Fig. 7; according to the previous diagram, it is observed that the quaternary catalyst activity in 2 M CH_3OH is the highest at current densities above 0.2–0.3 A cm^{-2}. The *IR*-free current–potential data for various catalysts in 2 M CH_3OH (Fig. 8) show that the overpotential is reduced in the presence of the quaternary catalyst (Pt:Ru–Sn–W = 1:1 molar ratio) electrode compared with the Pt–Sn/C, Pt–W/C and Pt–Ru/C electrodes prepared in similar conditions and having the same Pt/metal ratio of 1:1 (Fig. 8). The lowest rest potential was recorded for the Pt–Sn(1:1) electrode at 0.265 V versus NHE. The performance of the Pt–W (1:1) electrode appeared very poor, probably due to the high content of tungsten oxides on the catalyst surface blocking the Pt sites. Electrode–kinetic parameters for the Pt–Ru–Sn–W/C catalyst were obtained by Tafel analysis (Fig. 9) after correction of data for both ohmic drop and mass-transfer polarization. The results are shown in Table 2. Accordingly, the lowest Tafel slope was observed in 2 M CH_3OH solution whereas the exchange-current density increased with the methanol concentration, as expected. Assuming the charge-transfer coefficient close to 0.5, the Tafel data suggested that both one-electron and two-electron processes were involved in the rate-determining step. Yet, these observations could not be conclusive as the symmetry of the energy barrier for the charge transfer at the electrode–electrolyte interface is not known a priori [32]. As the reversible potential for methanol oxidation in acidic environments is 0.04 V(NHE) [33], it was derived from the Tafel analysis (Table 2) that the exchange-current density is higher in 5 M CH_3OH, whereas the Tafel slope is the lowest in a 2 M CH_3OH solution. This behaviour probably accounts for the different polarization characteristics at low and high currents observed in Fig. 7. Such an effect is probably determined by a large electrode flooding by methanol and a reduced water availability near the electrode surface in 5 M CH_3OH.

The Pt–Ru–Sn–W/C catalyst was used as the anode in a fuel cell test station. The cathode was a commercial Prototech gas-diffusion electrode (0.35 mg Pt cm^{-2}). The geometrical area of the electrodes was 5 cm^2 and both electrodes consisted of carbon cloth supports. The

Table 2
Electrode–kinetic parameters for methanol oxidation in sulfuric acid on a Pt–Ru–Sn–W/C catalyst at various methanol concentrations

Methanol concentration (mol/l)	Tafel data		Ohmic drop		Exchange-current density [b] (A cm^{-2})	Rest potential (V vs. NHE)
	Slope (mV/dec)	$n\alpha$	Experimental (Ω cm^2)	Calculated [a] (Ω cm^2)		
1 M	91.0	0.725	0.59	0.65	2.04×10^{-3}	0.3
2 M	87.6	0.753	0.57	0.62	2.57×10^{-3}	0.288
5 M	95.6	0.69	0.57	0.64	6.35×10^{-3}	0.277

[a] Determined by a least-square fitting of the polarization curves.
[b] Related to the geometrical electrode area.

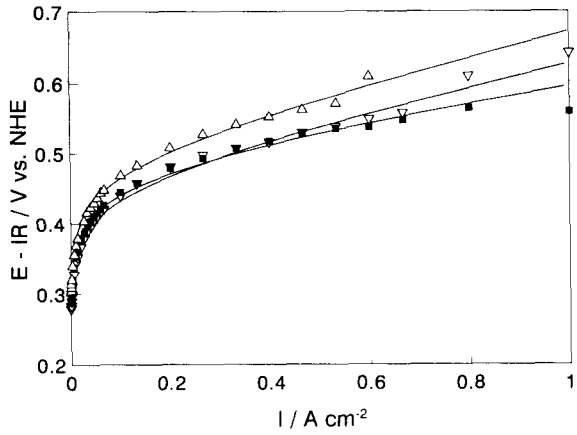

Fig. 7. *IR*-free polarization curves for the oxidation of methanol in 0.5 M H_2SO_4 at 60 °C at Pt–Ru–Sn–W/C electrodes: (△) 1 M; (■) 2 M, and (▽) 5 M.

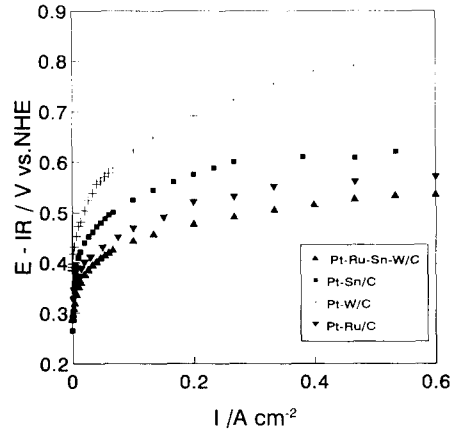

Fig. 8. *IR*-free polarization curves for the oxidation of methanol (2 M) in 0.5 M H_2SO_4 at 60 °C at various catalysts.

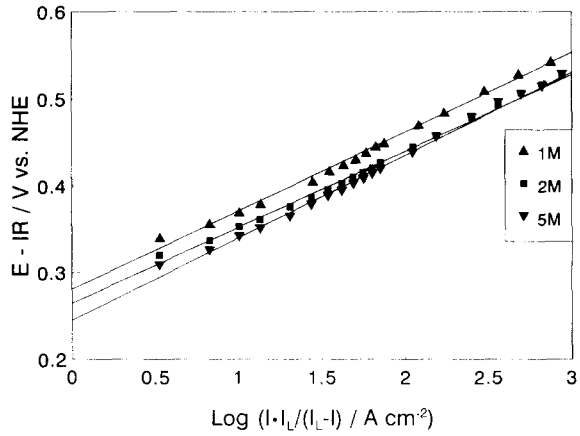

Fig. 9. Polarization curves upon correction of the data in Fig. 5 for both ohmic drop (*IR*) and mass-transfer polarization: full lines indicate the Tafel slopes.

Nafion membrane–electrode assembly was prepared by following the method described in Ref. [22]. It was observed that the Prototech cathode could substain a very high current for oxygen reduction with a small polarization in a proton-exchange membrane fuel cell [22, 34]. The cell was operated at 60 °C and atmospheric pressure for the methanol-fed anodic compartment and 5 bars for the oxygen pressure in the cathodic compartments. The cell was left in open-circuit condition with recirculating methanol solution and humidified oxygen, in order to reach the hydration equilibrium for the membrane. This was reflected by steady-state values for both the cell resistance (0.62 Ω cm^2) and the open-circuit voltage (OCV) value (0.63 V). Before the hydration equilibrium was reached, the cell resistance progressively decreased whereas a transient behaviour was observed for the open-circuit potential. The OCV reached a maximum of 0.75 V followed by a rapid decrease to a steady-state value of 0.63 V. The OCV was lower than the theoretical value calculated by the rest potentials of the cathode and anode in half-cells. Both transient behaviour and low OCV values accounted for a methanol cross-over effect. The methanol cross-over was confirmed by chromatographic analysis of the solution produced in the cathodic compartment. The cell showed a large activation polarization and significant ohmic losses (Fig. 10). The large cell polarization should be ascribed to both the poor anodic activity and the cathode poisoning by methanol cross-over. A significant decrease in the catalyst activity during the oxygen reduction was previously observed for Nafion-coated Pt/C electrodes exposed to methanol [35, 36], as reflected by a decrease in the rest potential and an increase in the Tafel slope [36].

These results show, at present, that the application of solid polymer electrolytes configuration to DMFCs needs significant improvements to confine methanol in the anode compartment and probably also to improve the CO_2 escape from the rear of the anode. It is also shown that the quaternary catalyst can deliver significant currents under the half-cell operation but, at same time, it can introduce some ohmic losses due to the presence of semi-insulating metal oxides (e.g., RuO_2, SnO_2, WO_3) limiting the single-cell performance.

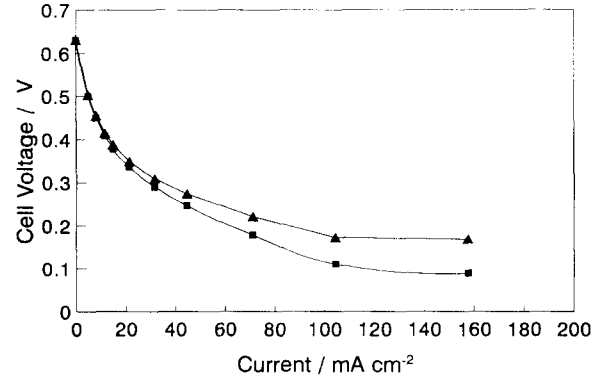

Fig. 10. Single-cell polarization curves for the Pt–Ru–Sn–W/C anode–Nafion electrolyte–Pt/C cathode assembly. (▲) *IR*-free polarization curve, and (■) observed polarization.

Acknowledgements

The authors are grateful to Mr Whanjin Roh (Department of Chemistry, Seoul National University) for his cooperation in the X-ray photoelectron spectroscopic analyses.

References

[1] M. Watanabe, S. Saegusa and P. Stonehart, *J. Electroanal. Chem., 271* (1989) 213.
[2] J.B. Goodenough, R. Manoharan, A.K. Shukla and K.V. Ramesh, *Chem. Mater., 1* (1989) 391.
[3] A. Hamnett, B.J. Kennedy and F.E. Wagner, *J. Catal., 124* (1990) 30.
[4] A.K. Shukla, M.K. Ravikumar, A. Roy, S.R. Barma, D.D. Sarma, A.S. Aricò, V. Antonucci, L. Pino and N. Giordano, *J. Electrochem. Soc., 141* (1994) 1517.
[5] A.S. Aricò, H. Kim, A.K. Shukla, M.K. Ravikumar, V. Antonucci and N. Giordano, *Electrochim. Acta, 39* (1994) 691.
[6] A. Aramata, I. Toyoshima and M. Enyo, *Electrochim. Acta, 37* (1992) 1317.
[7] K. Chandrasekaran, J.C. Wass and J.O'M. Bockris, *J. Electrochem. Soc., 137* (1990) 518.
[8] B. Beden, C. Lamy, A. Bewick and K. Kunimatsu, *J. Electroanal. Chem., 121* (1981) 343.
[9] R. Inada, K. Shimazu and H. Kita, *J. Electroanal. Chem., 277* (1990) 315.
[10] K.J. Cathro, *J. Electrochem. Soc., 116* (1969) 1608.
[11] M.M.P. Janssen and J. Moolhuysen, *Electrochim. Acta, 21* (1976) 869.
[12] M.M.P. Jansen and J. Moolhuysen, *J. Catal., 46* (1977) 289.
[13] M.M.P. Jansen and J. Moolhuysen, *Electrochim. Acta, 21* (1976) 861.
[14] B. Beden, F. Kadirgan, C. Lamy and J.M. Leger, *J. Electroanal. Chem., 127* (1981), 75.
[15] W. Vielstich, P.A. Christensen, S.A. Weeks and A. Hamnett, *J. Electroanal. Chem., 242* (1988) 327.
[16] M. Shibata and S. Motoo, *J. Electroanal. Chem., 209* (1986) 151.
[17] P.K. Shen and A.C.C. Tseung, *Ext. Abstr., Proc. 186st Meet. The Electrochemical Society, Honolulu, HI, USA, 16–21 May 1993,* Proc. Vol 93-1, Abstr. No. 576.
[18] P.K. Shen and A.C.C. Tseung, *Ext. Abstr., Proc. 186st Meet. The Electrochemical Society, Honolulu, HI, USA, 16–21 May 1993,* Proc. Vol. 93-1, Abstr. No. 8778.
[19] D.A. Shirley, *Phys. Rev. B, 5* (1972) 4709.
[20] C.D. Wagner, *J. Electron Spectrosc. Relat. Phenom., 32* (1983) 99.
[21] L.C. Feldman and J.W. Mayer, *Fundamentals of Surface and Thin Film Analysis*, North Holland, Amsterdam, 1986, pp. 226–228.
[22] E.A. Ticianelli, C.R. Derouin, A. Redondo and S. Srinivasan, *J. Electrochem. Soc., 135* (1988) 2209.
[23] A.S. Aricò, V. Antonucci, N. Giordano, A.K. Shukla, M.K. Ravikumar, A. Roy, S.R. Barman and D.D. Sarma, *J. Power Sources, 50* (1994) 295.
[24] M. Pourbaix, *Atlas of Electrochemical Equilibria in Aqueous Solutions*, Pergamon, London, 1966.
[25] A.N. Buckley and B.J. Kennedy, *J. Electroanal. Chem., 302* (1991) 261.
[26] C.D. Wagner, W.M. Riggs, L.E. Davis and J.F. Moulder, in G.E. Mullemberg (ed.), *Handbook of X-ray Photoelectron Spectroscopy*, Perkin-Elmer Corporation, Eden Prairie, MN, 1978.
[27] M. Peuckert, *Electrochim. Acta, 29* (1984) 1315.
[28] K.S. Kim, N. Vinograd and R.E. Davis, *J. Am. Chem. Soc., 93* (1974) 6296.
[29] W.M. Latimer, *The Oxidation States of the Elements and their Potential in Aqueous Solutions*, Prentice Hall, Englewood Cliffs, NJ, 1952, pp. 254–257.
[30] A.S. Aricò, A.K. Shukla, V. Antonucci and N. Giordano, *J. Power Sources, 50* (1994) 177.
[31] N. Sugumaran and A.K. Shukla, *J. Power Sources, 39* (1992) 249.
[32] A.J. Bard and L.R. Faulkner, *Electrochemical Methods: Fundamentals and Applications*, Wiley, New York, 1980.
[33] D.S. Cameron, B. Harrison and R.J. Potter, *Proc. CEC–Italian Fuel Cell Workshop, Taormina, Italy, 4–5 June 1987*, pp. 201–212.
[34] S. Surampudi, S.R. Narayanan, E. Vamos, H. Frank and G. Halpert, A. LaConti, J. Kosek, G.K. Surya Prakash and G.A. Olah, *J. Power Sources, 47* (1994) 377.
[35] W. Vielstich, A. Kuver, M. Krausa, A.C. Ferreira, K. Petrov and S. Srinivasan, *Proc. Symp. Batteries and Fuel Cells for Stationary and Electric Vehicle Applications*, The Electrochemical Society, Pennington, NJ, USA, 1993, pp. 269–280.
[36] A.S. Aricò, V. Antonucci, V. Alderucci, E. Modica and N. Giordano, *J. Appl. Electrochem., 23* (1993) 1107.